Journal of Thermal Analysis and Calorimetry (2020) 141:301–312
https://doi.org/10.1007/s10973-020-09319-1

Performance of ejector refrigeration cycle based on solar energy working with various refrigerants

Md Khairul Bashar Shovon[1] · Senthil Kumar Raman[1] · Abhilash Suryan[2] · Tae Ho Kim[1] · Heuy Dong Kim[1]

Received: 29 October 2019 / Accepted: 10 January 2020 / Published online: 23 January 2020
© Akadémiai Kiadó, Budapest, Hungary 2020

Abstract

The refrigerator unit based on electrically driven vapor compression technology consumes high energy, associated with high cost and loss of ecosystem. Recently, solar thermal energy emerges as a key research area and introducing it in refrigerator application has happened extremely fast. Solar thermal refrigeration systems based on ejector compression technology are thriving because of its utilization of low-grade energy sources, straight forward design, non-moving parts, lower maintenance costs, and durability. In this present work, the performance of a solar ejector refrigeration system (ERS) is calculated analytically using one-dimensional model. The performance parameters are calculated with the assumption that both the condensation and evaporation processes occur along the saturation line. Initially, the influence of the ejector area ratio, generator temperature, condenser temperature, and evaporator temperature on the performance of the ERS is analyzed in critical mode with water (R718) as the working fluid. The analysis shows that the coefficient of performance increases more than two times on increasing the ejector area ratio from 6.4 to 12.8. The results also show that a higher coefficient of performance (COP) is obtained at a higher ejector area ratio. The COP is found to be inversely related to the generator temperature, meanwhile the coefficient of performance increase more than 74% on increasing the refrigeration temperature from $T_c = 8$ °C to $T_c = 15$ °C. Then, the performance of ERS is obtained at the subcritical conditions at varying generator temperatures. At subcritical mode, COP is found to be directly proportional to the generator temperature, and the highest COP occurs at an optimum generator temperature. The performance of the ERS with various refrigerants as R717, R718, R245fa, R123, R141b, and R365fa is calculated at the critical mode. With refrigerant R717, the system shows higher performance as well as a cooling effect than other refrigerants. However, most environmental benign refrigerant R718 shows comparatively low performance, but it is found that R718 produces a significant cooling effect than other refrigerants excluding R717 refrigerant.

Keywords Low-grade energy · Renewable energy resources · Ejector refrigeration system · Entrainment ratio · Coefficient of performance

Introduction

The conventional compressor-based refrigeration system operates with CFCs causing ozone layer depletion and has large energy-consuming moving parts. This energy mostly extracts from non-renewable sources like fossil fuels. On the other hand, the cooling demand is increasing day by day, and continuous dependence on natural fuel contributes to CO_2 emissions into the atmosphere. Solar thermal refrigeration system (STRS) is a better alternative way which converts heat energy from the renewable energy source and waste heat sources and provides a cooling effect. Solar thermal energy emerges as a smart energy system that is cost-effective and 100% renewable energy system. Utilization of solar thermal energy in the refrigeration system conserves energy as well as reduces the global CO_2 footprint, and hence, this technology draws the interest of both the scientific community and industries [1]. Moreover, TRS is capable of operating a wide range of working fluids that are environmentally safe, non-toxic, nonflammable, and non-corrosive.

✉ Abhilash Suryan
suryan@cet.ac.in

✉ Heuy Dong Kim
kimhd@anu.ac.kr

1 Department of Mechanical Engineering, Andong National University, Andong, South Korea

2 Department of Mechanical Engineering, College of Engineering Trivandrum, Thiruvananthapuram, India

Based on the working principle, the thermal refrigeration system is classified into an absorption refrigeration system, adsorption refrigeration system, and ejector refrigeration system (ERS) [2]. Among these three types, an absorption refrigeration system can ensure a large cooling effect. However, it occupies a large installation area and requires high maintenance costs. The adsorption refrigeration system has low performance compared to the other two types. The ERS has the benefit of simplicity, reliability, no moving parts, low operational cost, and less maintenance cost [3]. Since ERS does not have any high power-consuming moving parts which ensure the advantage of the energy conservation and intrigues the reputation, low COP associated with the ERS is the main barrier to comprehensive applications. Therefore, continuous researches are ongoing to enhance the system performance of ERS under overall operating condition. In order to improve the performance of ERS, the knowledge about the influence of ejector geometry [4], operational condition [5], and working fluid is necessary [6].

Analytical modeling of ejector flow was initially developed by Keenan et al [7]. In their study, they asserted that flow through the ejector, primary and secondary flow begins to mixing at a constant pressure at the inlet of constant area section. Later, this hypothesis was adopted and modified in most of the theoretical studies [8, 9]. Munday and Bagster et al. [8] improved Keenan et al. mixing theory and asserted that the primary flow from nozzle exit does not mix with the secondary flow for a certain distance inside the constant area section called primary flow core. This diverging portion of the primary flow core forms as a converging section for the secondary flow and accelerates it to the sonic speed. Both the primary and secondary flows are chocked at this section, and then the ejector operates in a critical mode, whereas the downstream pressure of the ejector is called critical pressure. Huang et al. [9] validated Munday and Bagster et al. hypothesis through numerical analysis and experimental test on eight different ejector geometry with R141b as working fluids.

Recently, researchers experimentally and theoretically analyzed the performance of ERS with different working fluids. Chen et al. [10] studied the performance of an ERS under overall operation modes using R600, R600a, R152a, R1234ze, R134a, R430A, R245fa, and, R290 as refrigerants. Dahmani et al. [11] obtained optimum performance using R290, R152a, R600a, and R134a as refrigerants. Gil et al. [12] considered the performance of an ERS with R356mfc, RC318, R245fa, R245ca, R236ca, R236ea, acetone, benzene, cyclopentane, cyclohexane, and toluene as refrigerants. In their study, the loss coefficient of flow through the ejector was considered constant. Tashtoush et al. [13] experimentally tested the performance of an ERS at critical mode using the superheated primary stream of various refrigerants such as R600, R600a, R290, R141b, R717, R152a, R134a, and R123 and compared with theoretical results of Chen et al. [14]. Hernandez et al. [15] studied the behavior of an ERS with R600, R600a, R134a, R123, R290, and R152a as refrigerants and showed that the R290 as the working fluid has the highest COP, while the R123 has a lowest COP. Recently, Gill et al. [16] estimated the performance of an ERS with ethers and fluorinated ethers as working fluids. Optimum COP values were obtained for dimethyl ether (R-E170) and diethyl ether using a one-dimensional computer program approach based on Huang et al. model. In the earlier studies, most of the researchers have considered working fluid either with ODP larger than zero [17] or with high GWP values. Due to the high ODP and GWP values of some refrigerants, they are either banned or proposed for banning [18].

Environment-friendly refrigerants have the advantages of comparatively low GWP and nearly zero ODP potential [24, 25]. Hence, research and development activities are increasing in analyzing the influence of environment-friendly working fluids, and their use in refrigeration technologies is gaining much interest [26]. Ayse Ugurcan et al. [27] evaluated the system performance of an ERS with R134a, R1234ze, and R1234yf and showed that the optimum COP for R1234ze, and R134a are nearly equal as well as higher than R1234yf. Smierciew et al. [28] experimentally investigated the first prototype ERS with HFO-1234ze operated by low-grade heat energy. In this study, a group of refrigerants has been investigated in the ejector refrigeration system. Table 1. indicates the safety group, the global warming potential (GWP), and the ozone depletion point (ODP) and other thermodynamic properties of the various working fluids including R718, R141b, R245fa, R717, R123, and R365mfc. Nehdi [29] analyzed the performance of refrigeration systems with different environment-friendly refrigerants at various generator conditions and found that R717 provides better performance. Thus, earlier studies are only analyzed with a particular component of ERS and not considered the whole system.

Upto author's knowledge, comprehensive analysis of environmental benign refrigerant on the integrated ejector refrigeration system is limited [30, 31]. The purpose of this study is to investigate an ERS under the critical and subcritical operation mode and analyze the performance with various refrigerants. A one-dimensional analytical model-based isentropic relations of on mass, momentum, and energy equations are used to analyze the system performance. Ejector refrigeration system performance with environment-friendly refrigerants, including R718, R141b, R245fa, R717, R123, and R365mfc is investigated. The influence of entrainment ratio, critical condensing temperature, and generator temperature on the performance of an ERS is analytically investigated. Further, the effect of ejector area ratios is also analyzed.

Table 1 Thermodynamic properties of various refrigerants

Refrigerant	Molecular formula	Molecular weight/g mol^{-1}	Boiling point/°C	Stagnation temperature/°C	Critical pressure (absolute)/MPa	GWP	ODP	ASHRAE safety group
R141b[19]	C2H3FCl2	116.9	32	204.2	4.25	725	0.12	A2
R245fa [19]	C3H3F5	134	15	154	3.65	1030	0	B1
R717 [20]	NH3	17.03	−33.3	133	11.42	0	0	B22
R718 [21]	H2O	18.2	100	373.95	22.06	0	0	A1
R123 [22]	C2HF3Cl2	152.9	27.6	183.68	3.662	77	0.02	B1
R365mfc [23]	C4H5F5	148.07	40.2	186.85	3.27	782	0	Unknown

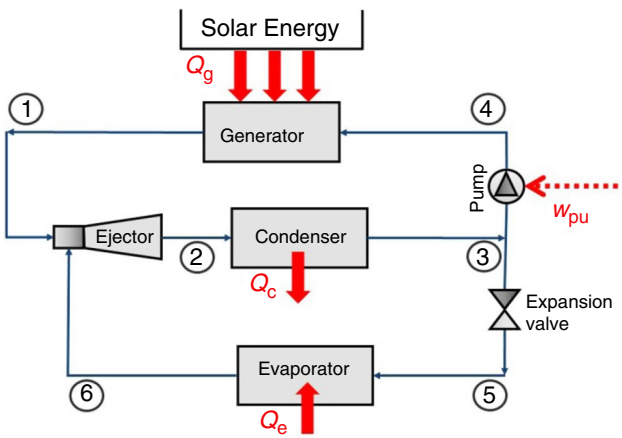

Fig. 1 Ejector refrigeration cycle

Ejector refrigeration cycle

A schematic representation of a simple ejector refrigeration system which encompasses a generator, an ejector, a condenser, an expansion valve, a feed pump, and an evaporator is shown in Fig. 1. Thermal energy procured from a low-grade heat source is supplied to the generator to vaporize the refrigerant fluid. Due to this vaporization process in a constant volume, the temperature of the primary flow (m_p) raises. The saturated pressure corresponding to this generator temperature (T_g) is considered as the generator pressure (P_g) of the primary flow. Then, the high pressurized primary flow enters into the ejector nozzle and expands and attains a sonic velocity at nozzle throat. The expansion continues in the diverging section of the primary flow core and attains a supersonic velocity with low-pressure, as shown in Fig. 2a. This low-pressure primary flow with high-velocity entrains the secondary flow (m_s) from the evaporator. The high-velocity of primary flow accelerates the secondary flow along the converging section formed due to the primary flow core to the sonic velocity at section *y–y*.

At section *y–y* in constant area section, the primary flow starts to mixes with the secondary flow at the same pressure. In here, there is a hypothetical throat in the constant area section, where the pressure of both primary and secondary flow is equal, and flow is chocked so that Mach value of secondary flow is unity as shown in Fig. 2b. After the hypothetical throat, the velocity of secondary flow increases downstream until section *m–m*, while the velocity of primary flow decreases. The velocity of both the primary and secondary flow attains the same supersonic value at the section *m–m*, and this mixed stream flows at supersonic speed till the section sh–sh where a shock wave occurs and becomes a subsonic flow. The pressure and velocity discontinuously rises and decreases, respectively, across the shock. The pressure of the subsonic mixed flow gradually increases as it discharges through the diffuser, and finally, it reaches the condenser pressure.

Once the mixed stream enters the condenser, rejects the heat (Q_c) and the steam condenses to a liquid at the condenser pressure. After this condensation, the liquid is separated into two flows. The first flow goes through the feed pump where pressure is increased to the generator level and the power loop 1–2–3–4–1 of the system cycle gets completed. The other part of the flow enters the expansion valve where the pressure is decreased to the evaporator level. After the expansion process, the flow enters the evaporator and absorbs heat. This heat absorption produces the necessary cooling effect (Q_e) of the refrigeration cycle and completes the refrigeration loop 2–3–5–6–2 of the system cycle.

Flow model

The ejector is a critical component of an ERS, and it significantly impacts the efficiency of the entire system. In this present work, Munday and Bagster et al. [8] hypothesis are adopted for modeling of the ejector system. The loss coefficients of the ejector are calculated as in Huang et al. [9] work. More details are presented in the section below.

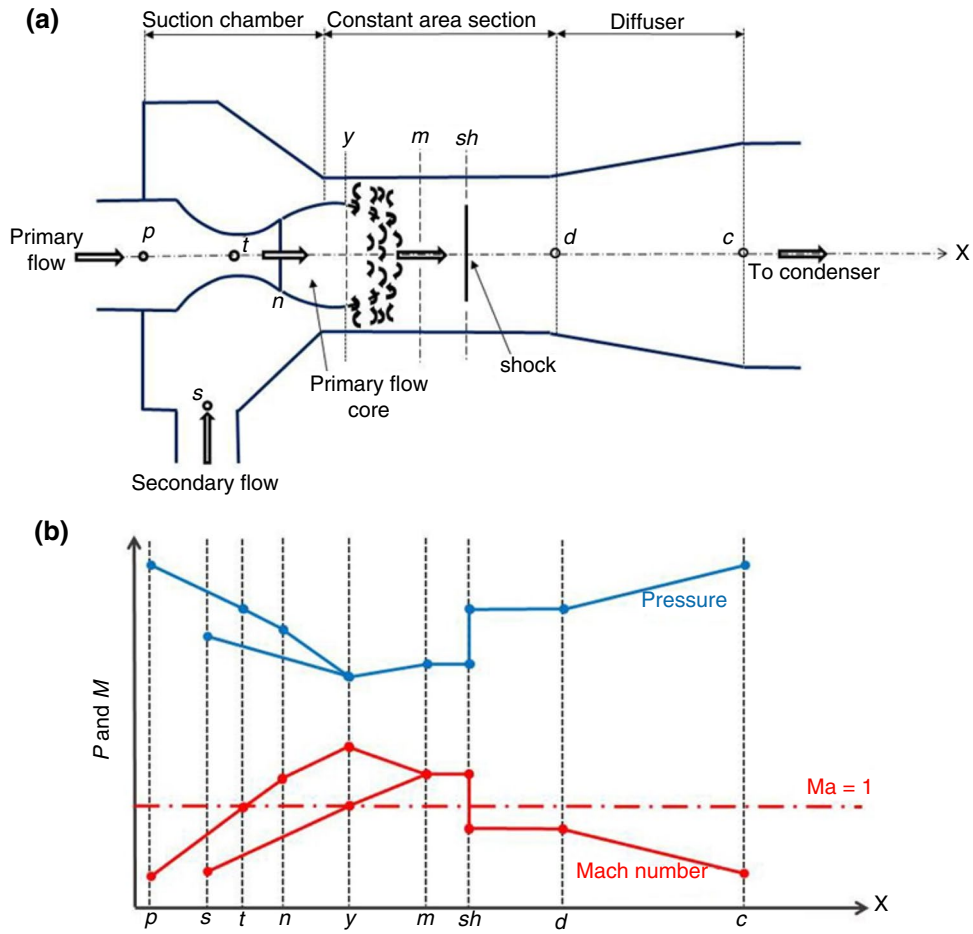

Fig. 2 Schematic representation of flow field in ejector and pressure Mach number distributions. **a** Flow field, **b** pressure and Mach number

Ejector

In this study, the following assumptions were adopted for the ejector as shown in Fig. 2.

1. The working fluid inside the system component is thermally perfect gas with temperature-dependent heat capacity ratio and enthalpy.
2. The flow through the entire system is steady state and one-dimensional.
3. The subcooling of condenser and superheating of evaporator flow are neglected, and for simplicity, flow is saturated vapors at the exit of the generator and evaporator, respectively.
4. The equation of flow through the ejector component is derived from the isentropic flow relation. But for avoiding the ideal process, mixing and frictional loss efficiencies are introduced in the isentropic relation.
5. Constant pressure mixing of the two-stream takes place inside the constant area section of the ejector.
6. Each component of the ejector refrigeration system is adiabatic control volume.

The mathematical equations for the ERS are given below:

Primary flow through nozzle

At the generator outlet, for a given generator temperature (T_g), and its corresponding saturated pressure (P_g), the primary mass ow rate (m_p), through the nozzle inlet is obtained by gas dynamic relation shown in Eq. 1,

$$m_p = \frac{P_g \times A_t}{\sqrt{T_g}} \times \sqrt{\frac{k}{R}\left(\frac{2}{k+1}\right)^{\frac{(k+1)}{(k-1)}}}\sqrt{\eta_p} \tag{1}$$

where the value of the isentropic coefficient for nozzle efficiency (η_p) = 0.95.

At the nozzle exit, the Mach number (M_{pn}) and pressure (P_{pn}) are obtained from the gas dynamics theory as expressed in Eqs. 2 and 3.

$$\left(\frac{A_{pn}}{A_t}\right)^2 = \frac{1}{M_{pn}^2}\left[\frac{2}{k+1}\left(1+\frac{k-1}{2}M_{pn}^2\right)\right]^{\frac{(k+1)}{(k-1)}} \tag{2}$$

$$\frac{P_g}{P_{pn}} = \left[1 + \frac{k-1}{2} M_{pn}^2\right]^{\frac{k}{(k-1)}} \tag{3}$$

Flow in the primary flow core

Since the primary stream covers a certain distance between section *n–n* and *y–y* without mixing with the secondary stream. The Mach value of M_{py} can be calculated from the isentropic relation mentioned in Eq. 4.

$$\frac{P_{py}}{P_{pn}} = \left[\frac{1 + \frac{k-1}{2} M_{pn}^2}{1 + \frac{k-1}{2} M_{py}^2}\right]^{\frac{k}{(k-1)}} \tag{4}$$

The area of the primary flow core, A_{py}, at section *y–y* is calculated from Eq. 5:

$$\left(\frac{A_{py}}{A_{pn}}\right)^2 = \frac{(\eta_{py}/M_{py})}{(1/M_{pn})}\left[\frac{\frac{2}{k+1}\left(1 + \frac{k-1}{2} M_{py}^2\right)}{\frac{2}{k+1}\left(1 + \frac{k-1}{2} M_{pn}^2\right)}\right]^{\frac{(k+1)}{2(k-1)}} \tag{5}$$

where the isentropic loss coefficient of primary flow in that section *y–y* (η_{py}) is considered as 0.88.

Secondary flow through the inlet to section *y–y*

For the critical operational mode, the secondary flow reaches the chocked condition at section *y–y*, and the Mach value of the secondary flow becomes a unity, i.e., $M_{sy} = 1$. For a total pressure (P_e) at the evaporator exit, the critical pressure of the secondary flow at this location is obtained from Eq. 6.

$$\frac{P_e}{P_{sy}} = \left[1 + \frac{k-1}{2} M_{sy}^2\right]^{\frac{k}{(k-1)}} \tag{6}$$

Then, the calculation of the secondary mass flow rate (m_s) at the critical operational mode can be done by using Eq. 7.

$$m_s = \frac{P_e \times A_{sy}}{\sqrt{T_e}} \times \sqrt{\frac{k}{R}\left(\frac{2}{k+1}\right)^{\frac{(k+1)}{(k-1)}}}\sqrt{\eta_s} \tag{7}$$

where the value of the isentropic coefficient related to secondary flow (η_s) is considered as 0.85.

During the subcritical mode operation, the velocity of the secondary flow at the section *y–y* is less than the sonic speed, i.e., $M_{sy} < 1$. Eqs. 8–11 are derived from the isentropic relationships of mass and energy conservation.

$$\frac{T_{sy}}{T_e} = \left[\frac{P_{sy}}{P_e}\right]^{\frac{k-1}{k}} \tag{8}$$

$$P_{sy} v_{sy} = R T_{sy} \tag{9}$$

$$V_{sy} = \sqrt{2C_p\left(T_e - T_{sy}\right)} \tag{10}$$

$$m_s = \frac{V_{sy} \times A_{sy}}{T v_{sy}}\sqrt{\eta_s} \tag{11}$$

The active area (A_d) calculated as the sum of the area of the primary stream, A_{py}, and the area of the secondary stream, A_{sy}, as shown in Eq. 12.

$$A_d = A_{py} + A_{sy} \tag{12}$$

Temperature at section *y–y*

The critical temperature of the primary and secondary flow at this section *y–y* is calculated from Eqs. 13 and 14:

$$\frac{T_g}{T_{py}} = 1 + \frac{k-1}{2} M_{py}^2 \tag{13}$$

$$\frac{T_e}{T_{sy}} = 1 + \frac{k-1}{2} M_{sy}^2 \tag{14}$$

Mixed flow before shock wave (section *m–m*)

The primary and secondary flow starts to mix from section *y–y*. A momentum and energy balance equations of the mixed flow are written as in Eqs. 15 and 16:

$$\phi_m\left(m_p V_{py} + m_s V_{sy}\right) = \left(m_p + m_s\right) V_m\right) \tag{15}$$

$$m_p\left(C_P T_{py} + \frac{V_{py}^2}{2}\right) + m_s\left(C_P T_{sy} + \frac{V_{sy}^2}{2}\right) = \left(m_p + m_s\right)\left(C_P T_m + \frac{V_m^2}{2}\right) \tag{16}$$

where V_m is the mixed flow velocity and the frictional loss coefficient, $\phi_m = 0.75$. V_{py} and V_{sy} are the primary and secondary flow velocities at section *y–y* as mentioned in Eqs. 17–20.

$$V_{py} = M_{py} \times a_{py} \tag{17}$$

$$a_{py} = \sqrt{k R T_{py}} \tag{18}$$

$$V_{sy} = M_{sy} \times a_{sy} \tag{19}$$

$$a_{sy} = \sqrt{kRT_{sy}} \tag{20}$$

The Mach value of the mixed flow is written as in Eq. 21

$$M_m = \frac{V_m}{a_m} \tag{21}$$

where a_m is the local speed of sound and calculated as in Eq. 22

$$a_m = \sqrt{kRT_m} \tag{22}$$

A sharp pressure increase occurs in the mixed flow due to the formation of a shock wave. After experiencing the shock, it is assumed that the mixed flow follows an isentropic process with constant pressure, P_d, inside the constant area section. The gas dynamic relations between section *m–m* to section *d–d* are written as in Eq. 23 and 24:

$$\frac{P_d}{P_m} = 1 + \frac{2k}{k+1}\left(M_m^2 - 1\right) \tag{23}$$

$$M_d^2 = \frac{1 + \frac{k-1}{2}M_m^2}{kM_m^2 - \left(\frac{k-1}{2}\right)} \tag{24}$$

Mixed flow through the diffuser (section *d–d*)

Assuming that the mixed flow through the diffuser undergoes an isentropic compression process with the pressure at the diffuser exit (P_{c*}) is written as in Eq. 25:

$$\frac{P_{c*}}{P_d} = \left[1 + \frac{k-1}{2}M_d^2\right]^{\frac{k}{(k-1)}} \tag{25}$$

Coefficient of performance (COP)

The state point 1, 2, and 6 represents the flow as the ejector primary flow, ejector secondary flow, and ejector outlet flow, respectively, as shown in Fig. 3.

The total amount of solar energy input in the generator is computed using Eq. 26.

$$Q_g = m_g\left(h_1 - h_4\right) \tag{26}$$

The total amount of mass flow rate passes through the condenser is computed as the sum of primary flow rate and secondary flow rate of the ejector as in Eq. 27.

$$m_c = m_s + m_p \tag{27}$$

The total amount of heat transfer rate through the condenser is computed from Eq. 28.

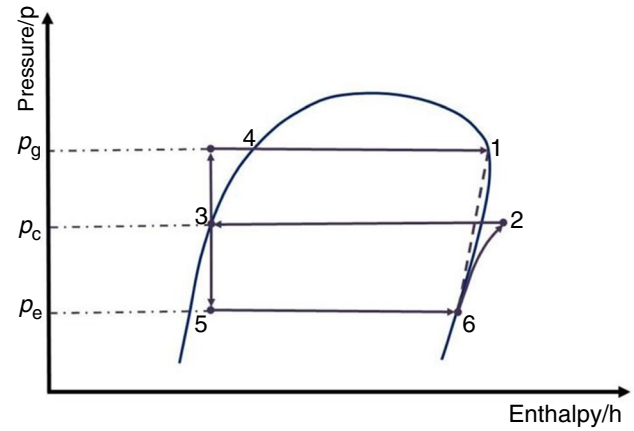

Fig. 3 Pressure-enthalpy diagram of the ejector refrigeration cycle

$$Q_c = m_c\left(h_3 - h_2\right) \tag{28}$$

Since the expansion process is isenthalpic, the enthalpy value is considered as a constant during the throttling process in the expansion valve as in Eq. 29.

$$h_3 = h_5 \tag{29}$$

Actual enthalpy of the flow after the pump work is computed from Eq. 30,

$$h_4 = h_3\frac{h_{4,is} - h_3}{\eta_{pu}} \tag{30}$$

Here, h_4 is calculated with the pressure at state point 1 and entropy at state point 3 in Fig. 3. The total amount of heat transfer rate through the evaporator is computed from Eq. 31.

$$Q_e = m_s\left(h_6 - h_5)\right) \tag{31}$$

Since the pump work of a liquid pump is much lower and can be overlooked in COP approximation in Eq. 32.

$$\mathrm{COP} = \frac{Q_e}{Q_g} = \frac{m_s\left(h_6 - h_5\right)}{m_p\left(h_1 - h_4\right)} = \mu\frac{\left(h_6 - h_5\right)}{\left(h_1 - h_4\right)} \tag{32}$$

Calculation procedure

Based on the equations mentioned in the earlier section, a computer program for solving the one-dimensional analytical modeling is developed in Scilab. The schematic representation of the flowchart is shown in Fig. 4.

The total temperature at the inlet of primary flow (T_g) and the secondary flow (T_e) is defined at a particular area

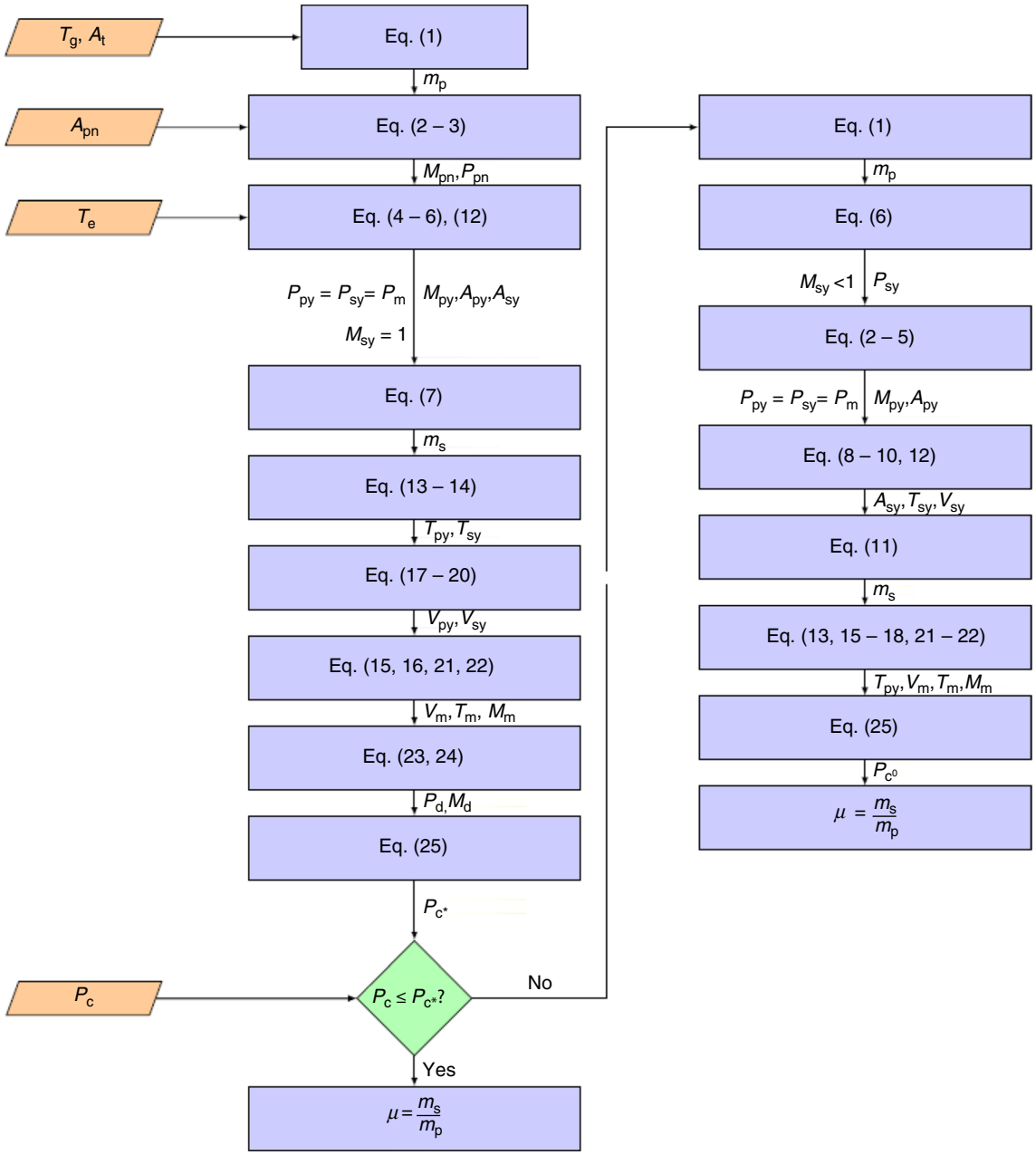

Fig. 4 Solution flowchart for ejector flow

ratio (AR). The ratio between ejector constant area (A_d) to the nozzle throat area (A_t) is defined as the area ratio. The corresponding saturated pressures P_g, P_e are calculated from the thermodynamic library coolprop using the python interface. The critical pressure (P_{c*}) is calculated by solving the series of equations from 1 to 25. If the $P_c \leq P_{c*}$, then flow through the ejector is considered as chocked and the critical performance parameters are calculated. For the condenser pressure, $P_c > P_{c*}$ the subcritical performance characteristics are calculated as in the right side of the flowchart. In a similar manner, the performance parameters are calculated at different ejector geometries by varying the area ratio from 6.4 to 12.8. During the analysis of performance with different refrigerants, the material properties are calculated from the thermodynamic library coolprop, and the same procedure is repeated.

The one-dimensional analytical solution is compared with the existing literature by Huang et al. [9] at critical operating conditions with saturated generator temperature ranges from 78 to 95 °C, evaporator temperature of 8 °C, and ejector area ratio of 8.28. However, in Fig. 5,

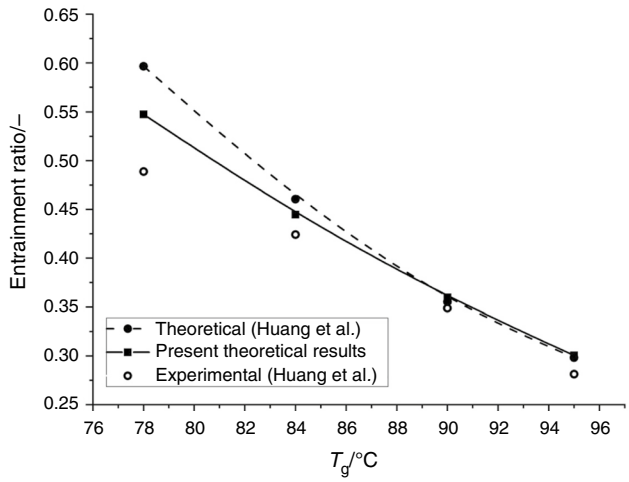

Fig. 5 Comparison of present results with the experimental and theoretical results of Huang et al

the present analytical solution shows good accuracy with experimental and theoretical analysis of Huang et al.

Results and discussion

Ejector refrigeration system under overall mode

The performance of an ERS with R718 as refrigerant is analyzed at both the subcritical and critical mode and presented in this section. At a fixed temperature of $T_e = 12$ and $T_c = 28$, the coefficient of performance is calculated at a varying T_g for different ejector area ratios as depicted in Fig. 6. On keeping the area ratio constant and increasing the T_g, the COP increases up to an optimum T_g, and then the COP starts to decrease. On keeping the T_c constant, at lower values of T_g, the ejector is operating in the subcritical mode of operation. On increasing the T_g value, the ejector flow becomes chocked and eventually, COP begins to gradually decrease. For instance, at point A in Fig. 6, AR = 12.8, $T_c = 28$ and $T_g = 50$. The corresponding P_c and P_g values are 3.783 kPa and 12.352 kPa, respectively. For this geometric and operational conditions, the critical pressure P_{c*} is calculated as 1.853 kPa. Therefore, at point "A," the $P_c > P_{c*}$, the mode of operation is subcritical and the COP increases with T_g. On further increment in T_g, P_{c*} the value becomes equal to P_c and the flow becomes chocked at point "B." After the point "B," the COP begins to decrease due to increment in T_g in critical mode.

As the AR decreases, the flow entertainment decreases, and hence, the COP also decreases. At a constant T_c, the critical pressure slightly increases with a decrease in the value of AR. Hence, the chocking point slightly decreases, which is reflected as decrement in the optimum T_g with decreasing AR.

Ejector refrigeration system under critical mode

Performance of the ejector refrigeration system using R718 as refrigerant is analyzed at critical mode under distinct operating conditions in this section.

At $T_g = 70$ °C, the values of entrainment ratio (μ) are calculated as a function of area ratio for various T_e as illustrated in Fig. 7. The ratio between the secondary mass flow rate (m_s) to primary mass flow rate (m_p) is defined as the entrainment ratio. On keeping the T_e constant and increasing the area ratio, increases the cross-section area of the ejector constant mixing section as well as the hypothetical throat area. This area increment allows for more primary flow with

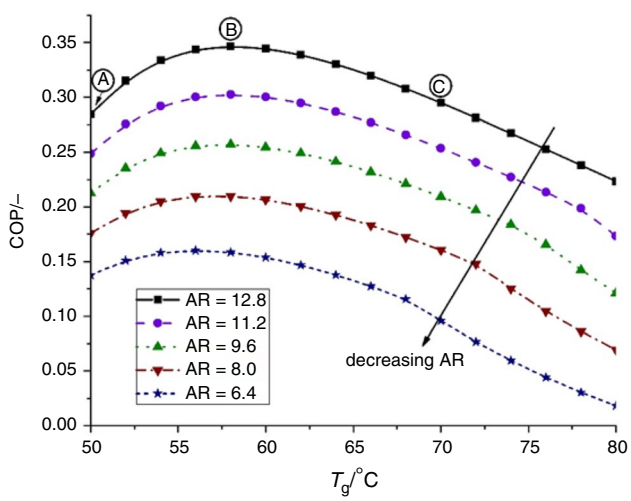

Fig. 6 Coefficient of performance at varying generator temperatures for different area ratios (R718, $T_e = 12$ °C and $T_c = 28$ °C)

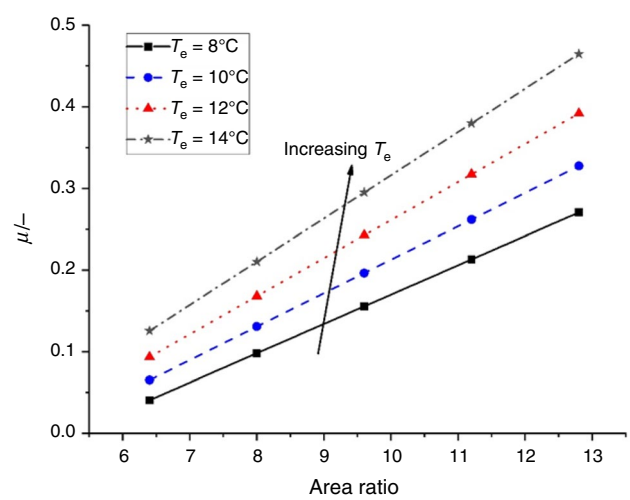

Fig. 7 Critical entrainment ratio at varying area ratios for different evaporator temperatures (R718, $T_g = 70$ °C)

an increased velocity which entrains higher secondary flow. Thus, the entrainment ratio increases with area ratio. As the T_e increases, the total inlet pressure at the secondary flow inlet increases which impose more secondary flow into the mainstream and eventually increases the ratio of m_s to m_p at a higher rate. Since the COP is a function of the entrainment ratio, the COP is also raised at a higher area ratio as depicted in Fig. 8.

At $T_e = 12$ °C, the values of critical entrainment ratio are calculated as a function of generator temperature for various area ratio as shown in Fig. 9. The higher T_g of primary flow corresponds to a higher P_g results in a higher primary mass flow rate. This higher rate of primary flow occupies more area in the constant area mixing section and allows only a small amount of the secondary mass flow. This reduction in the secondary mass flow from the evaporator results in lowering of entrainment ratio values with increasing T_g. Further, continuous increment in the T_g for a particular area ratio completely blocks the secondary flow from entraining into the constant area section and results in a zero entrainment ratio. Figure 9 also shows that zero entrainment condition occurs at lower generator temperature for smaller area ratio relative to larger area ratio cases. For instance, the value of entrainment ratio approaches nearly close to zero at the generator temperature approximately 81 °C or higher. This phenomenon occurs at much higher generator temperature for the higher ejector area ratios. The COP also follows a similar trend with area ratio under the critical operational mode, as shown in Fig. 10.

Under the ejector critical operating condition, the condensing pressure is less than the critical pressure. Therefore, at a constant T_e, the COP is found to be nearly invariant with the T_c, as shown in Fig. 11. As the T_e increases, the total pressure at the secondary inlet increases and imposes higher

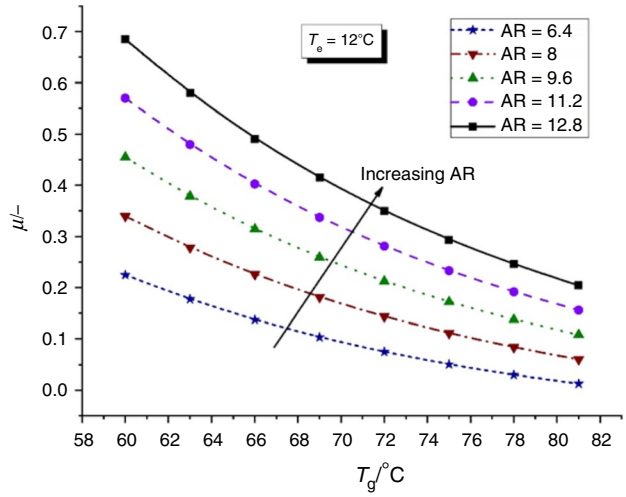

Fig. 9 Critical entrainment ratio at varying generator temperatures for different area ratios (R718, T_e= 12 °C)

secondary flow into the constant area mixing section, which results in more entrainment ratio and COP.

The influence of evaporator temperature on the ejector entrainment ratio and system performance at various generator temperatures is illustrated in Figs. 12 and 13, respectively. As seen earlier, under the critical mode of ejector operation, the higher evaporator temperature corresponds to high total pressure at the secondary inlet. Hence, more secondary flow streams into the constant area mixing section at the same primary flow results in higher entrained mass flow rate, and the system shows better performance. As the generator temperature increases result in higher primary mass flow rate and decrease the secondary mass flow rate

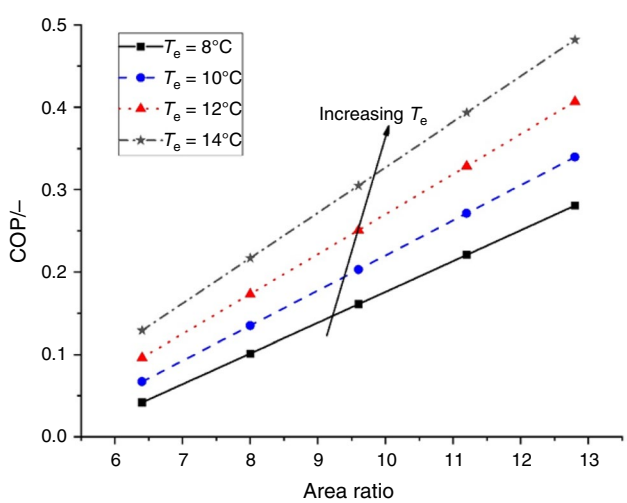

Fig. 8 Critical coefficient of performance at varying area ratios for different evaporator temperatures (R718, T_g= 70 °C)

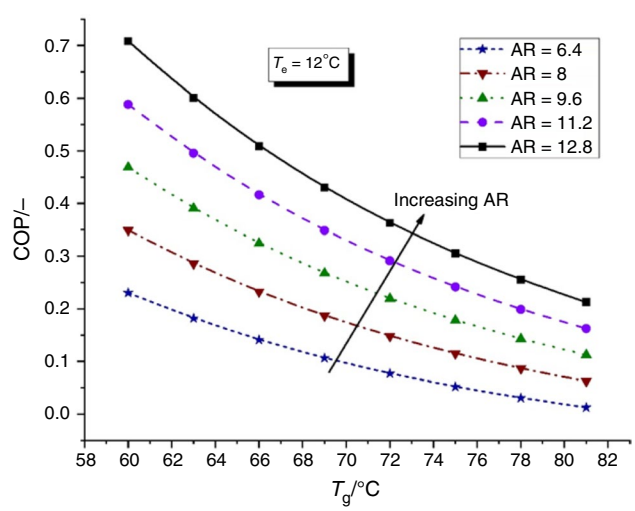

Fig. 10 Critical coefficient of performance at varying generator temperatures for different area ratios (R718, T_e= 12 °C)

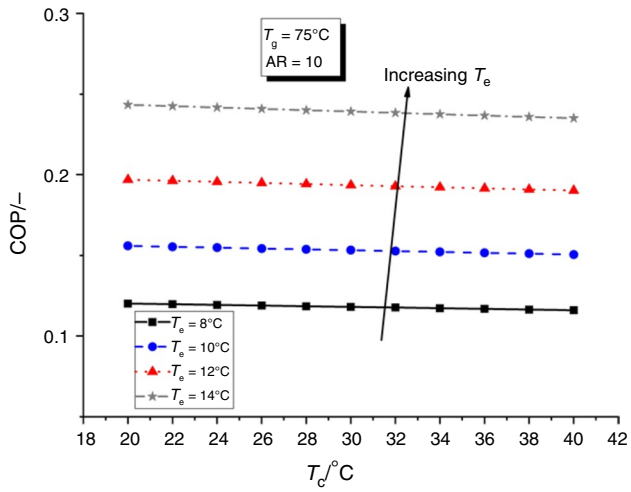

Fig. 11 Critical coefficient of performance at varying condenser temperatures for different evaporator temperatures (R718, T_g = 75 °C and AR = 10)

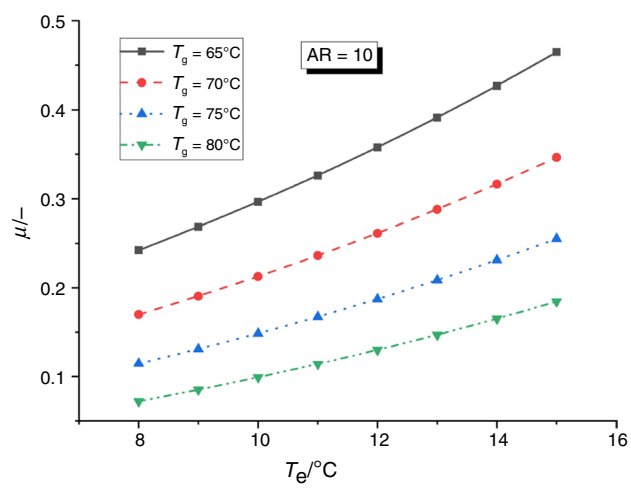

Fig. 12 Critical entrainment ratio at varying evaporator temperatures for different generator temperatures (R718 and AR = 10)

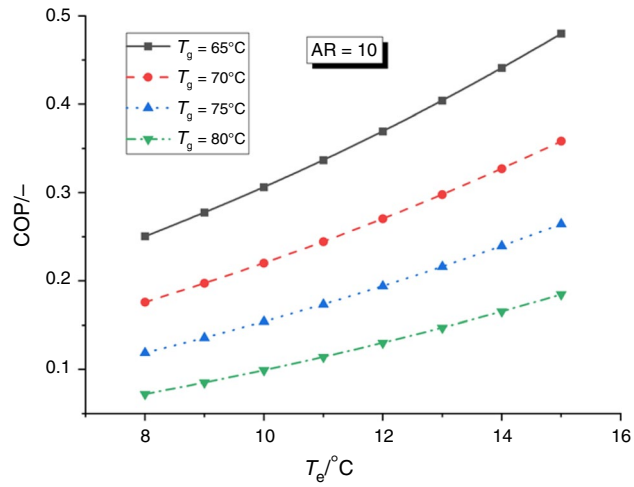

Fig. 13 Critical coefficient of performance at varying evaporator temperatures for different generator temperatures (R718 and AR = 10)

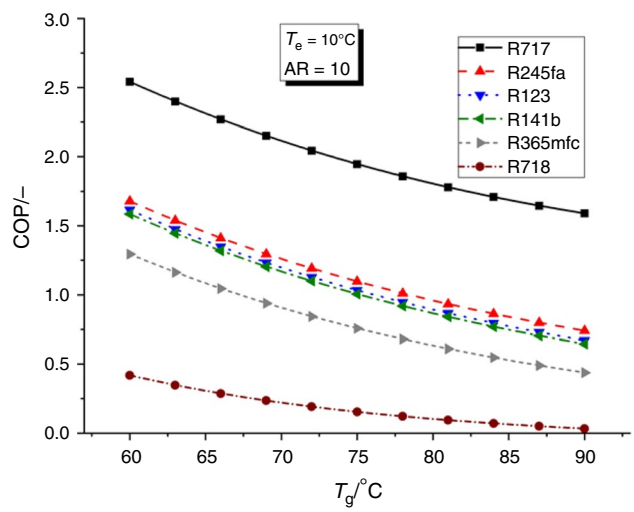

Fig. 14 Critical coefficient of performance at varying generator temperatures for different refrigerants (T_e = 10 °C and AR = 10)

to be entrained from the evaporator, therefore, at T_e = 8 °C and T_g = 80 °C, the values of entrainment flow and COP approach to zero.

Ejector refrigeration system using various refrigerants

The different behaviors of the ejector refrigeration system using R718 as refrigerant have already been reviewed in Sect. 5.1. As given in Table 1, some other commonly used refrigerants are set to compare under ejector critical mode of operation.

The coefficient of performance (COP) of the system for different refrigerants is determined at varying generator temperature, as shown in Fig. 14. The COP lessens with an increase in the generator temperature as seen earlier for the case of R718 refrigerants. However, all the refrigerants show better performance than the R718, while the R717 exhibits greater improvement in the performance at AR = 10 and T_e = 10 °C. The different thermodynamic properties of each refrigerant are tabulated in Table 2.

On keeping the AR and T_g as constant and increasing the T_e, the COP gets increased, as shown in Fig. 15. Under the ejector critical condition, continuous increasing in evaporator temperature gives higher entrainment ratio and COP. However, the performance dramatically varies with different working fluids, and particularly R717 shows substantial enhancement in the performance. The enthalpy h_6 increases

Table 2 Material properties of different refrigerants

Refrigerants	C_p/kJ kg^{-1} K^{-1}	k	R/kJ kg^{-1} K^{-1}
R717	4.699	1.799	488.2×10^{-3}
R718	1.986	1.33	456.813×10^{-3}
R141b	0.908	1.145	71.09×10^{-3}
R245fa	1.075	1.152	62.022×10^{-3}
R123	0.79	1.135	54.375×10^{-3}
R365mfc	1.139	1.091	56.138×10^{-3}

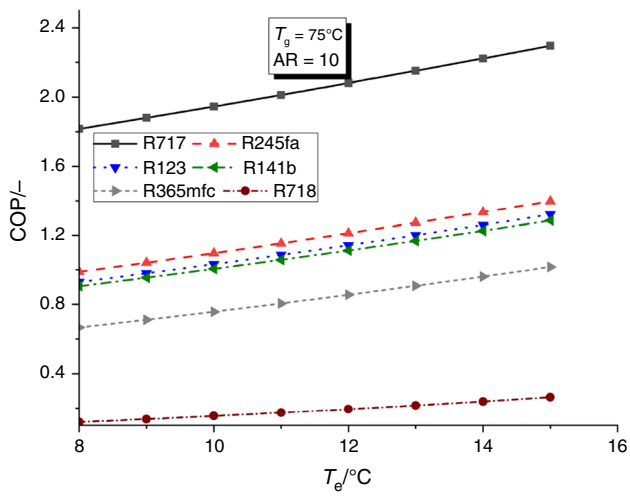

Fig. 15 Critical coefficient of performance at varying evaporator temperatures for different refrigerants (T_g = 75 °C and AR = 10)

continuously at higher evaporative temperature; thus, latent heat of vaporization upraises as in Fig. 3.

The cooling load of per unit mass of refrigerant represents the ratio of $Q_e/(m_p+m_s)$ and the consumption of refrigerant declines with an increase in cooling load. So, it will be cost-effective because the investment behind the refrigerants will moderate [20], and the cooling load of different refrigerants is shown in Fig. 16. The R717 establish superior performance with the highest cooling load of more than twice as the R718. Even though the R141b, R245fa, R123, and R365mfc showed a better COP and entrainment ratio than R718, their cooling load is three times lower than the R718.

In the ejector refrigeration system, COP is an important index but not the only reason. In that situation, the environmental impact created by the refrigerant should consider. The detail is already discussed in Sect. 1. As shown in Fig. 16, the order of the refrigerants follows as: R717 > R718 > R141b > R245fa > R123 > R365mfc. In spite of having a larger cooling load, R717 is not a wise decision because it is toxic in nature. Using nonflammable gas R141b and R123 will be a good choice as a replacement of R717, but they have ODP greater than zero. Moreover, R245fa and R365mfc have zero ODP, but their GWP is not considerable.

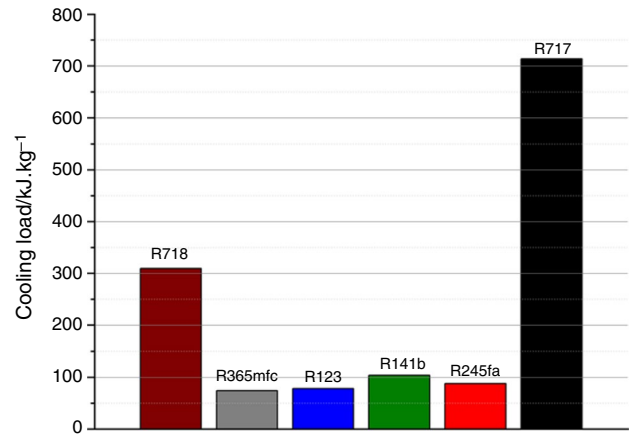

Fig. 16 Cooling load comparison between different refrigerants

Besides having low COP, R718 has no environmental impact and is suggested in this study.

Conclusions

A one-dimensional theoretical analysis of the ejector refrigeration system working with low-grade energy resources is presented in this present work. A computer program based on a series of isentropic relations of ejector flow is developed in Scilab and interfaced with coolprop, a thermodynamic library, for material properties of different working fluids. Initially, the performance of the ejector refrigeration systems is calculated under the overall operation mode. Later, the system performance is evaluated with different refrigerants under critical mode.

Before the subcritical mode of operation, at a constant area ratio and condenser pressure, the coefficient of performance increases with an increase in the generator temperature until the chocking condition. At the chocking condition, the generator temperature attains an optimum value and gives the highest COP. This COP value ranges from 0.25 to 0.17 at a given area ratio of 11.2 under overall mode. In the critical mode, further increment in generator temperature diminishes the performance.

Under the critical mode operation, at a constant generator temperature as well as a constant evaporator temperature, increasing the area ratio widens the hypothetical throat area and allows more secondary flow and enhances the performance. Increasing the evaporator temperature strengthens the secondary flow and imposes more secondary flow into the constant area mixing section. In contrast, increasing the generator temperature increases the primary flow and stalls the secondary flow. Thus, the increment in evaporator temperature enhances the system performance while the

increment in generator temperature diminishes the system performance.

Among the six considered refrigerants, R717 exhibits substantially better performance in terms of entrainment ratio, coefficient of performance, and cooling load. Even though the R718 shows the least coefficient of performance and entertainment ratio, it shows moderate cooling capacity than R141b, R245fa, R123, and R365mfc.

Acknowledgement This work was supported by a Research Grant of Andong National University.

References

1. Ullah KR, Saidur R, Ping HW, Akikur RK, Shuvo NH. A review of solar thermal refrigeration and cooling methods. Renew Sustain Energy Rev. 2013;24:499–513. https://doi.org/10.1016/j.rser.2013.03.024.
2. Sarbu I, Sebarchievici C. Review of solar refrigeration and cooling systems. Energy Build. 2013;67:286–97. https://doi.org/10.1016/j.enbuild.2013.08.022.
3. Wang F, Shen S. Energy and exergy analysis of novel solar bi-ejector refrigeration system with injector. Int J Energy Res. 2009;34(9):815–26. https://doi.org/10.1002/er.1602.
4. Aphornratana S, Chungpaibulpatana S, Srikhirin P. Experimental investigation of an ejector refrigerator: effect of mix- ing chamber geometry on system performance. Int J Energy Res. 2001;25(5):397–411. https://doi.org/10.1002/er.689.
5. Ma X, Zhang W, Omer SA, Riffat SB. Performance testing of a novel ejector refrigerator for various controlled conditions. Int J Energy Res. 2011;35(14):1229–35. https://doi.org/10.1002/er.1766.
6. Elhub B, Aziz MAA, Mat MKABS. Proceedings of the 8th international conference on renewable energy sources and proceedings of the 2nd international conference on environmentalinformatics, Kuala Lumpur, Malaysia April 23–25, 2014; ISSN: 2227-4359, ISBN: 978-960-474-370-4.
7. Keenan JH, Neumann EP. A simple air ejector. J Appl Mech Trans ASME. 1942;64:75–81.
8. Munday JT, Bagster DF. A new ejector theory applied to steam jet refrigeration. Ind Eng Chem Process Des Dev. 1997;16(4):442–9.
9. Huang BJ, Chang JM, Wang CP, Petrenko VA. 1-D analysis of ejector performance. Int J Refrig. 1999;22(5):354–64. https://doi.org/10.1016/S0140-7007(99)00004-3.
10. Chen J, Havtun H, Palm B. Screening of working fluids for the ejector refrigeration system. Int J Refrig. 2014;47:1–14. https://doi.org/10.1016/j.ijrefrig.2014.07.016.
11. Dahmani A, Aidoun Z, Galanis N. Optimum design of ejector refrigeration systems with environmentally benign fluid. Int J Therm Sci. 2011;50(8):1562–72. https://doi.org/10.1016/j.ijthermalsci.2011.02.021.
12. Gil B, Kasperski J. Efficiency analysis of alternative refrigerants for ejector cooling cycles. Energy Convers Manag. 2015;94:12–8. https://doi.org/10.1016/j.enconman.2015.01.056.
13. Tashtoush B, Alshare A, Al-rifai S. Performance study of ejector cooling cycle at critical mode under superheated primary flow. Energy Convers Manag. 2015;94:300–10. https://doi.org/10.1016/j.enconman.2015.01.039.
14. Chen W, Liu M, Chong D, Yan J, Blair A, Bartosiewicz Y. A 1D model to predict ejector performance at critical and sub-critical operational regimes. Int J Refrig. 2013;36(6):1750–61. https://doi.org/10.1016/j.ijrefrig.2013.04.009.
15. Hernandez JI, Roman R, Best R, Dorantes R, Gonzalez HE. The behavior of an ejector cooling system operating with refrigerant blends 410A and 507. Energy Procedia. 2014;57:3021–30. https://doi.org/10.1016/j.egypro.2014.10.338.
16. Gil B, Kasperski J. Performance estimation of ejector cycles using ethers and fluorinated ethers as refrigerants. Appl Therm Eng. 2017;2018(133):269–75. https://doi.org/10.1016/j.applthermaleng.2018.01.061.
17. Sun DW, Eames IW. Performance characteristics of HCFC-123 ejector refrigeration cycles. Int J Energy Res. 1996;20(10):871–85. https://doi.org/10.1002/(SICI)1099-114X(199610)20:10%3c871:AID-ER201%3e3.0.CO;2-4.
18. Handbook for the montreal protocol on substances that deplete the ozone layer, Twelfth edition. Ozone Secretariat, United Nations Environment Programme, Nairobi, Kenya, 2018.
19. Bellos E, Tzivanidis C. Optimum design of a solar ejector refrigeration system for various operating scenarios. Energy Convers Manag. 2017;154(September):11–24. https://doi.org/10.1016/j.enconman.2017.10.057.
20. Chen W, Shi C, Zhang S, Chen H, Chong D, Yan J. Theoretical analysis of ejector refrigeration system performance under overall modes. Appl Energy. 2017;185:2074–84. https://doi.org/10.1016/j.apenergy.2016.01.103.
21. Kumar M. Study of water as a refrigerant and compare it with other current working refrigerants. Int J Innov Res Technol. 2015;2(7):426–36.
22. Calm JM, Hourahan GC. Refrigerant data update. Heat Pip Air Cond Eng. 2007;79(January):50–64.
23. Abdalla ME. Exergy performance of the environmentally friendly refrigerant mixture: R365mfc and R152a. Int J Res Appl Sci Eng Technol: IJRASET. 2015;3(I):47–59.
24. Kopchick S, Scancarello M. New refrigerants designation and safety classifications. 2017.
25. Pavel M, Rahmatollah K, Björn P. R1336mzz-Z—new generation non-fammable low GWP refrigerant; Energy Technology-KTH, Technical Report, 2019; pp. 1–8.
26. Alexis GK. Exergy analysis of ejector-refrigeration cycle using water as working fluid. Int J Energy Res. 2005;29(2):95–105. https://doi.org/10.1002/er.1042.
27. Ayse Ugurcan A, Erek A, Ekren O. Investigation of new generation refrigerants under two different ejector mixing theories. Energy Procedia. 2017;136:394–401. https://doi.org/10.1016/j.egypro.2017.10.271.
28. Smierciew K, Gagan J, Butrymowicz D, Łukaszuk M, Kubiczek H. Experimental investigation of the first prototype ejector refrigeration system with HFO-1234ze (E). Appl Therm Eng J. 2017;110:115–25. https://doi.org/10.1016/j.applthermaleng.2016.08.140.
29. Nehdi E, Kairouani L, Elakhdar M. A solar ejector air-conditioning system using environment-friendly working fluids. Int J Energy Res. 2008;32(13):1194–201. https://doi.org/10.1002/er.1413.
30. Riffat SB, Omer SA. CFD modelling and experimental investigation of an ejector refrigeration system using methanol as the working fluid. Int J Energy Res. 2001;25(2):115–28. https://doi.org/10.1002/er.666.
31. Sarkar J. Geometric parameter optimization of ejector-expansion refrigeration cycle with natural refrigerants. Int J Energy Res. 2010;34(1):84–94. https://doi.org/10.1002/er.1558.

Publisher's Note Springer Nature remains neutral with regard to jurisdictional claims in published maps and institutional affiliations.